

# Inverse Compton X-rays from strong FRII radio-galaxies

G. Brunetti<sup>1,2</sup>, G. Setti<sup>1,2</sup>, and A. Comastri<sup>3</sup>

<sup>1</sup> Dipartimento di Astronomia, via Zamboni 33, I-40126 Bologna, Italy

<sup>2</sup> Istituto di Radioastronomia del CNR, via Gobetti 101, I-40126 Bologna, Italy

<sup>3</sup> Osservatorio Astronomico di Bologna, via Zamboni 33, I-40126 Bologna, Italy

December 2, 2024

**Abstract.** In the framework of the quasars–radio galaxies unification the radio-emitting lobes of FRII radio galaxies are pervaded by an intense quasar radiation field. Inverse Compton (IC) scattering between the relativistic electrons and the IR–optical photons from a hidden quasar may provide an important contribution to the X-ray emission of these radio galaxies. The soft X-ray emission properties of six strong, high redshift FRIIs (3C 277.2, 280, 294, 324, 356, 368) are compared with our model expectations, taking into account also the contribution from the IC scattering of the CMB photons with the radio electrons. Our estimates are based on a *typical* quasar spectrum, derived from the infrared and optical properties of a 3C quasar sample, and on the assumption of energy equipartition between relativistic particles and magnetic fields with the same energy density in the electron and proton components and with a fixed low energy cut-off in the particle distribution (Appendix A).

We find that the soft X-ray luminosities and spectra of five out of six sources can be satisfactorily explained by our model with the exception of 3C 324 whose X-ray emission is probably dwarfed by that of the galaxies’ cluster of which this source is a member.

In the case of 3C 277.2 our model requires a luminosity of the hidden quasar which is in perfect agreement with that derived from spectropolarimetric studies. In order to carry out the computations of the IC scattering of the hidden quasar photons, which are propagating radially outward, we have solved the anisotropic IC problem. The formal approach and relevant formulae, which do not appear to be available in the literature, are presented in the Appendix B. One important effect is the prediction that the observed X-ray emission associated with the two radio lobes would be asymmetric if the radio axis is inclined with respect to the plane of the sky, the far-away lobe being the more luminous. The ratio between the X-ray luminosities of the two lobes is derived for several values of the inclination of the radio axis. However, the predicted

*Send offprint requests to:* G. Brunetti, Istituto di Radioastronomia, Via Gobetti 101, 40129 Bologna, Italy

angular sizes of these distant radio galaxies are small and difficult to be resolved with present X-ray facilities.

**Key words:** Radiation mechanism: non-thermal — Scattering — Galaxies: active — quasars: general — X-rays: general

## 1. Introduction

There is a growing evidence that radio-loud quasars and powerful radio galaxies with FRII radio structure belong to the same population. According to Barthel (1989) the quasar phenomenon shows up whenever the line of sight to the source happen to be within about 45 degrees from the radio axis, while at larger viewing angles the quasar is obscured by a surrounding thick torus of molecular gas co-axial with the radio axis. Indeed, X-ray observations of the archetypal radio galaxy Cygnus A have shown that the nuclear source is well described by a heavily absorbed ( $N_H = 3.7 \times 10^{23} \text{ cm}^{-2}$ ) power law spectrum with energy index  $\alpha \simeq 1$  and an intrinsic isotropic luminosity (2 – 10 keV) of  $\simeq 10^{45} \text{ erg s}^{-1}$ , both these figures being typical of the X-ray properties of steep spectrum radio-loud quasars (Arnaud et al. 1987; Ueno et al. 1994). In addition, the recent detection of a broad, but relatively weak, Mg II emission line typical of quasars from this narrow-line radio galaxy (NLRG) can be convincingly interpreted as the signature of a hidden quasar whose light is being scattered into the line of sight by gas clouds in the host galaxy (Antonucci et al. 1994). Similarly, the discovery of broad Mg II emission lines from several NLRGs indicates the presence of a hidden quasar in these sources (di Serego Alighieri et al. 1989; Dey & Spinrad 1996; Cimatti et al. 1993, 96).

A compilation of data obtained with the *Einstein* Observatory shows that the X-ray luminosities of FRII radio galaxies in the 0.3 – 3.5 keV interval are comprised in the

range  $10^{41-45}$  erg s $^{-1}$ , with the broad-line radio galaxies (BLRG) being the more luminous ones (Fabbiano et al. 1984), as expected in the unification model. ROSAT PSPC pointed observations have now revealed several low redshift BLRGs whose X-ray emission (unresolved) is consistent with intrinsically absorbed spectra (Allen & Fabian 1992; Crawford & Fabian 1995). At one extreme there is the well known case of 3C 109 ( $z \simeq 0.3$ ) whose spectrum is consistent with an absorbed power law of energy spectral index  $\alpha \sim 0.8$  ( $N_H = 5 \times 10^{21}$  cm $^{-2}$ ) and an unabsorbed luminosity (0.1-2.4 keV) of  $\simeq 5.6 \times 10^{45}$  erg s $^{-1}$ .

While these results generally support the unification scheme relating the FRII radio galaxies to the radio-loud quasars, nevertheless detailed studies of the X-ray properties of distant radio galaxies are made difficult due to the emission of the hot intracluster gas in which they might be embedded. Indeed, it has been shown that distant powerful radio galaxies tend to lie at the centre of moderately rich clusters (Hill & Lilly 1991; Yates et al. 1989).

In the case of Cygnus A, and because of its nearness ( $z = 0.057$ ), it has been possible to disentangle part of the X-ray structure of the radio galaxy despite the powerful emission ( $\sim 10^{45}$  erg s $^{-1}$ ) associated with the surrounding hot cluster gas. ROSAT HRI observations have revealed two high brightness emission regions, coincident with the radio hot spots, whose intensities can be explained as Inverse Compton (IC) scattering of the radio photons by the relativistic electrons in the hot spots themselves (Harris et al. 1994a). The evidence for a source centered on the nuclear region of the galaxy has been found by subtracting a King model in the ROSAT HRI frame (Harris et al. 1994b) and has been confirmed by GINGA observations (Ueno et al. 1994) revealing the presence of an absorbed powerful AGN type power law in the X-ray spectrum of Cygnus A. The source can be represented by an unresolved component, but there appears to be some extended emission present in the measuring circle of radius 10'' (Harris et al. 1994b). ROSAT HRI observations of the Cygnus A region have also revealed significant departures in the X-ray brightness distribution from a simple modified King model which have been interpreted as the signature of the hydrodynamic interaction of the jets/lobes with the hot cluster gas (Carilli et al. 1994).

The X-ray detections of several others, but more distant ( $z \sim 1$ ) powerful NLRGs have been generally interpreted as due to the emission of a hot intracluster gas either because their spectra do not show any evidence of intrinsic absorption (3C 356; Crawford & Fabian 1993) or because by analogy with Cygnus A the absorbed nuclear sources would be too weak to be detected at large distances (3C 277.2, 368; Crawford & Fabian 1995).

In this paper we point out that significant fluxes of X-rays are produced in the radio lobes of strong radio galaxies by the IC process. Recently, Feigelson et al. (1995) have reported the detection of soft X-rays (ROSAT PSPC) from the radio lobes of the nearby radio galaxy Fornax A

and argued that the surface brightness is consistent with that expected from the IC scattering of the cosmic microwave background (CMB) photons with the relativistic electrons in the lobes under conditions of energy equipartition between particles and magnetic fields, the relativistic electrons and protons having equal energy densities. These conclusions have been strengthened by the observations made with ASCA GIS (Kaneda et al. 1995). It is well known that the production of X-rays by this mechanism increases with the redshift since the CMB photon density is  $\propto (1+z)^3$ . On the other hand, in the framework of the unification scheme, the radio lobes are pervaded by an intense radiation flux from the misdirected hidden quasar and the ensuing IC losses roughly outweigh those due to the CMB whenever  $L_{46} \geq R_{100}^2(1+z)^4$ , where  $L_{46}$  is the isotropic luminosity of the quasar in units of  $10^{46}$  erg s $^{-1}$  and  $R_{100}$  is the distance from the quasar in units of 100 Kpc.

In Sect.2 we shall discuss the main assumptions of our model, while the results of its application to six high redshift radio galaxies, for which X-ray data are available, will be presented in Sect.3. The basic IC formulae required by our model are derived and discussed in the Appendix B. In this paper  $H_0 = 75$  km s $^{-1}$  Mpc $^{-1}$  and  $q_0 = 0.0$  are assumed throughout.

## 2. Model Assumption

### 2.1. Radiation spectrum of the hidden quasars

Of course one doesn't know what are the radiation properties of the hidden quasars. We know, however, that quasars' continuum spectra from the far IR to the optical can be roughly approximated by a power law [ $F(\nu) \propto \nu^{-\alpha}$ ] with  $\alpha \sim 1$ . From the standpoint of the IC computation the far- and near-IR emissions are of particular importance. Based on studies of various statistical samples (Sanders et al. 1989; Heckman et al. 1992, 94) we have adopted a *typical* quasar continuum spectrum as a combination of several power laws:  $\alpha = 0.2, 0.9, 1.7$  and  $0.6$  respectively in the intervals  $100 - 50\mu\text{m}$ ,  $50 - 6\mu\text{m}$ ,  $6000 - 650\text{nm}$  and  $650 - 350\text{nm}$ . It should be immediately stressed that a precise knowledge of these quantities is not critical for the computation of the IC emissivities to be discussed later on. The *typical* spectrum is anchored to the mean rest frame luminosity ( $50-6\mu\text{m}$ ) of the 3CR quasar's sample of Heckman et al. (1994) and to the mean optical luminosity ( $650-350\text{ nm}$  rest frame) for the same objects derived from their V magnitudes (Spinrad et al. 1985) assuming a spectral index  $\alpha = 0.6$ . The quasar sample span a redshift range from 0.3 to 2.0 with an average  $z \sim 1$ . We find that the integrated isotropic luminosity of the *typical* high redshift radio-loud quasar is  $L_{<Q>} = 9.5 \times 10^{46}$  erg s $^{-1}$ . The corresponding absolute magnitude is  $M_V \sim -26.1$ . We shall refer to the luminosity of this *typical* quasar in our estimates of the IC contri-

bution to the X-ray flux of distant radio galaxies due to the scattering of the photons from a hidden quasar.

In agreement with Barthel's unified scheme we adopt the view that a radio-loud quasar is surrounded by a thick dusty torus coaxial with the radio structure and with a half opening angle of 45 degrees. Accordingly we shall assume that only the relativistic electrons located within the quasar emission cone are those involved in the IC scattering of the quasar photons. However this is strictly the case for the optical photons only. Studies of various statistical samples (Heckman et al. 1992, 1994) suggest that the mean far/near-IR emission of quasars is 4-5 times greater than that of FRII radio galaxies, which might be interpreted either as re-radiation of a sizeable part of the emission from an extended thick dusty torus (Pier & Krolik 1992) or as a combination of thermal (isotropic) and non-thermal (anisotropic) nuclear radiation (Hes et al. 1995). Therefore, by assuming the same spatial distribution for both optical and far/near-IR photons, we shall neglect any possible additional IC contributions from electrons located outside the quasar emission cone.

## 2.2. Relativistic particles and equipartition fields

We assume that the radio lobes contain a uniform distribution of relativistic electrons and protons with equal energy density and that there exist an approximate equipartition between the particle and magnetic field energy densities (minimum energy condition). The radio lobe spectra can be generally described by power laws, with typical spectral index  $\alpha_R = 0.8$ , produced by the synchrotron process of ultra-relativistic electrons having a differential power law energy distribution ( $\propto K_e \gamma^{-\delta}$ ) with  $\delta = 2\alpha_R + 1$ . The strengths of the equipartition fields,  $B_{eq}$ , are normally computed with reference to the observed radio flux densities in a given frequency interval, say 10 MHz – 100 GHz source frame (e.g. Pacholczyk 1970). Since the synchrotron emission at a frequency  $\nu$  is mainly contributed by the electrons with a Lorentz factor  $\gamma \sim 5 \cdot 10^2 [\nu(\text{MHz})/B_\perp(\mu\text{G})]^{1/2}$ , then the lower bound in this frequency interval corresponds to  $\gamma = 10^3 - 10^4$  for typical  $B_{eq} = 1 - 10 \mu\text{G}$  and, as a consequence, a large fraction of the energy associated with the relativistic particles may reside at lower  $\gamma$ 's.

On the other hand, electrons with Lorentz factor  $\gamma \sim 100 - 200$  are precisely those which are required to produce X-rays via IC scattering of the IR-optical photons of the quasar radiation field. Of course, the modification of the equipartition quantities induced by the presence of these particles at lower energies may be readily estimated with the standard equipartition formulae by imposing a low frequency cut-off significantly smaller than the usually adopted 10 MHz, say 10–100 KHz in the source frame. On the other hand, by choosing the same value of the low frequency cut-off for sources with different  $B_{eq}$  strengths one would obtain different lower bound in the energy distri-

bution of the particles. In order to avoid this formal complication, we have applied equipartition equations based on a low energy cut-off ( $\gamma_{min}$ ) in the particle distribution (Appendix A).

For a comparison of the model predicted IC contribution with the observed soft X-ray flux from a source it is important to determine the shape of the electron spectrum at low energies where ionization losses may become relevant. In a completely ionized gas the ionization losses equal those due to the combined synchrotron and Compton processes at

$$\gamma_* \simeq \frac{3.5 \cdot 10^2 \sqrt{n_e}}{B_{-5}} \sqrt{78 - \log(n_e)} \quad (1)$$

where  $n_e$  is the density of thermal electrons and  $B_{-5} = (B_{eq}^2 + B_C^2)^{1/2}$  in units of  $10^{-5}$  gauss with  $B_C$  the equivalent field for Compton losses. Since the time dependence of the ionization losses is  $\propto \gamma$ , by solving the particle energy continuity equation (Kardashev 1962) one finds that the power law distribution should flatten by one unit in the exponent, that is  $\delta - 1$ , for  $\gamma < \gamma_*$ . At large redshifts  $B_{-5} > 2.5$  and with  $n_e < 10^{-3} \text{ cm}^{-3}$  one finds  $\gamma_* < 40$ . From the Faraday depolarization studies of high redshift FRIIs with one-sided jets Garrington & Conway (1991) have derived central values (halo models) of the  $n_e B$  product of about  $40 \times 10^{-3} \text{ cm}^{-3} \mu\text{G}$ , while  $n_e B < 5 \times 10^{-3} \text{ cm}^{-3} \mu\text{G}$  in the radio lobes, under the assumption that the depolarization is due to thermal gas within the sources. Then it can be safely assumed that in general  $n_e < 5 \times 10^{-4}$  in the radio-lobes. As a consequence, we shall adopt  $\gamma_* = \gamma_{min} = 20$  and, accordingly, use Eq.(A3) to compute the equipartition quantities. If it were  $\gamma_* > 20$  the strength of the equipartition field so derived would be an upper limit, the normalization of the electron spectrum would be lower (Appendix A), and the computed X-ray emission would be underestimated (typically by  $\sim 5 - 15\%$ ). However, if  $\gamma_*$  is significantly greater than 150, then the number of low energy electrons involved in the scattering of the quasar IR photons would be too much depleted and, consequently, our estimates of the IC soft X-ray flux would be overestimated.

As a first approximation we assume that the energy density of the relativistic particles in the radio lobes remains constant with time. The spatial distribution of the low energy electrons, which mainly contribute to the soft X-ray flux by the IC scattering of a *typical* quasar IR radiation field, cannot be directly inferred from radio observations. From the distribution of the low frequencies brightness profiles of powerful radio galaxies (Leahy et al. 1989; Carilli et al. 1991), it seems reasonable to assume that these particles are distributed approximately with an ellipsoidal geometry centered around the galaxy's nuclear region and circumscribing the high frequency radio lobes, i.e. the site of the ultra-relativistic particles with shorter radiative lifetimes.

On the other hand, synchrotron and Compton losses steepen the power law distribution of the electrons by one unit in the exponent. Several results (Alexander & Leahy 1987; Leahy et al. 1989) suggest that, in general, the corresponding steepening of the radio spectra occurs at high frequencies ( $\geq 1.5$ GHz), i.e.  $\gamma \geq 10^4$  for typical equipartition fields. Nevertheless, one can not exclude that for the oldest parts of the radio galaxies the high frequency spectral break has actually been shifted to very low frequencies. As a consequence for each source we have computed the equipartition quantities with reference to the observed flux at low frequencies (178 MHz), assumed to be emitted by the whole volume describing a radio source (prolate ellipsoid), in which case the derived synchrotron emissivity should be considered as a lower limit, leading to a lower limit on the normalization of the electron spectra.

### 2.3. Inverse Compton estimates and main model dependences

First of all, if the radiation field is mainly contributed by the hidden quasar and the surrounding dusty torus, a very small region compared with the size of a radio galaxy, then the associated photon momenta are distributed anisotropically. On the other hand the formula for the IC process have been normally derived under the assumption of a locally isotropic distribution of both electrons and photons momenta (Blumenthal & Gould 1970; Rybicki & Lightman 1979). Basically, the same results are found in our model when considering the total IC luminosity from a radio galaxy, and the associated spectral shape, due to the assumed geometry, i.e. the symmetric spatial distribution of the relativistic particles and the wide half opening angle ( $45^0$ ) of the quasar emission cone. However, by removing the hypothesis of a locally isotropic distribution of the photons' momenta, the computed IC luminosity depends strongly on the angle between the line of sight and the momenta of the incident photons from the nuclear region. By solving the anisotropic IC equations it is possible to derive the ratio between the X-ray luminosities of the two radio lobes. This ratio depends mainly on the inclination of the radio axis on the plane of the sky, but it also depends on the assumed geometry (half opening angle of the quasar radiation cone) and on the spectral energy distribution of the electrons (Fig.4 & 5 in the Appendix B). In principle the X-ray luminosity ratio of the two radio lobes is a direct observable and it could be combined with the radio depolarization data to constrain the geometry of the system.

For a given value of the electron spectral slope  $\delta$ , the IC contribution from a hidden quasar to the soft X-ray flux of a radio galaxy ( $L_Q^{IC}$ ) is proportional to  $K_e$ , to the total quasar luminosity  $L_Q$  and, roughly, to the cubic root of the radio galaxy volume. A compendium of data (Herbig & Readhead 1992) shows that the radio luminosities of FRII radio galaxies span a wide range from  $10^{42}$  to  $10^{45}$

erg s $^{-1}$ . Since optical and (extended) radio luminosities of steep spectrum radio quasars appear to be well correlated (Browne & Murphy 1987), one can predict that in the framework of the unification model the most powerful radio galaxies should also provide the strongest contribution to  $L_Q^{IC}$ .

In the case of the hidden quasar model it is straightforward to roughly describe the expected X-ray brightness profile: while the quasar photon density decreases with the square of the distance ( $r^{-2}$ ), the column density of the relativistic electrons along the line of sight within the quasar emission cone increases with  $r$ , so that the brightness distribution is  $\propto r^{-1}$  and consequently the luminosity of a shell at a distance  $r$  from the nucleus is roughly constant. However, at large distances (several tens Kpc) the quasar emission cone intercepts the ellipsoidal surface enclosing the particle distribution, so that the column density of scattering electrons along the line of sight starts decreasing and, as a consequence, a systematic decrease of the luminosity profile as a function of distance is expected (see Fig.1).

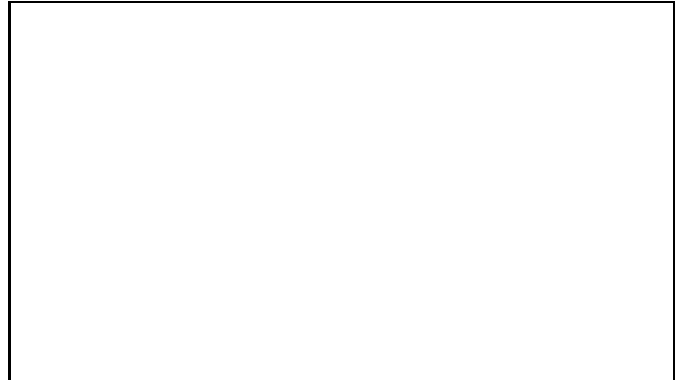


**Fig. 1.** The predicted (normalized) IC X-ray luminosity of the radio galaxy 3C 280, assumed to lie on the sky plane (symmetrical lobes). The relativistic particles are uniformly distributed in the volume bounded by the quasar radiation cone and the ellipsoidal surface from the 1.4 GHz radio maps. The luminosity profile is obtained by integrating the surface brightness distribution over circular arcs at a distance  $r$  from the nucleus. The total luminosity profile (solid line) is the sum of the contribution from the IC scattering of the hidden quasar photons (dotted line) and of those of the CMB (dashed line). The contribution of the "CMB" to the total luminosity is  $\sim 10\%$ . The radio lobes of the 5 GHz map extend inward to  $\sim 15$  Kpc, while those of the 1.4 GHz map reach the nuclear region (Ronghui et al. 1992).

In addition to the quasar model, the contribution to the X-ray flux from the IC scattering of the CMB photons in powerful radio galaxies may become increasingly important with the redshift, the IC emissivity being  $\propto (1+z)^{\frac{\delta+5}{2}}$  (e.g. Blumenthal & Gould 1970). The density of the CMB

photons is constant throughout the radio source volume and the photons' momenta are locally isotropic. Given the much softer spectrum of the CMB the relativistic electrons responsible for a given X-ray IC emission are on the average more energetic than those required in the IC scattering of the hidden quasar radiation field. The contribution to the soft X-ray flux from each source has been estimated by applying standard formulae in the literature (e.g., Harris & Grindlay 1979) to our source model.

The estimates of the IC fluxes depend, other things being equal, on the assumed orientation of the radio axis. Let the angle between the line of sight and the radio axis be  $\theta_{ax}$  (Fig.4 in the Appendix B). The volume of a radio galaxies (assumed to be ellipsoidal) is roughly  $\propto (\sin \theta_{ax})^{-1}$ , so that from the synchrotron emissivity formula and from Eq.(A3) it is found that the contribution to the IC flux from the scattering of the CMB photons is  $\propto (\sin \theta_{ax})^{-\frac{\delta+1}{\delta+5}}$ , i.e. it increases with decreasing  $\theta_{ax}$ . The dependence on the inclination angle of the IC flux from the scattering of the quasar radiation field cannot be evaluated with simple geometrical considerations. Taking into account the dilution of the quasar photon field one would find that for an elongated ellipsoidal distribution the IC flux roughly decreases with  $\theta_{ax}$  as  $(\sin \theta_{ax})^{\frac{\delta+9}{\delta+5}}$ , but this is more than compensated by the enhanced IC emission of the far radio lobe (Fig.4 in the Appendix B).

While, on the one hand (Sect. 2.2), the adopted source volumes lead to lower limits for the synchrotron emissivity and the normalization of the electron spectra, on the other hand it might be argued that the total number of the relativistic particles in the radio galaxies are overestimated, thus leading to an overestimate of the derived X-ray luminosities. It should be stressed, however, that this effect might be relevant only in the case of the IC scattering with the CMB photons, but not in the case of the IC scattering of the quasar photons, for which the electrons responsible of the scattering are only those located within the quasar emission cone. If the particles are uniformly distributed within an ellipsoidal volume of minor axis  $b$ , then it can be shown with simple geometrical considerations that, under equipartition conditions, the luminosity due to IC scattering of the hidden quasar photons goes as  $b^{\frac{2\delta-5}{7}}$ , while that of the CMB photons as  $b^{\frac{2(\delta+1)}{7}}$ . For instance, with  $\delta = 2.6$  a change of  $b$  by a factor 3 (i.e. a factor 9 in the volume) means a change of a factor  $\sim 3$  in the predicted X-ray luminosity from the IC scattering of the CMB photons, but only  $\sim 10\%$  in that predicted by the IC scattering of the quasar photons.

It should be noted, however, that the minor axis  $b$  in our source models is not a free parameter. It is derived by fitting the outer contours of the high-frequency radio lobes of each source. Therefore, from the standpoint of the present discussion it might be more appropriate to consider an alternative situation where particles and fields are uniformly distributed only in that part of the ellip-

soidal volume intercepted by the quasar radiation cones. In this case the reduction in the volume implies an increase in the equipartition particle density (eq.A3) and, consequently, an increase in the predicted X-ray flux from the IC scattering of the quasar photons with respect to the uniformly filled ellipsoidal volume model. This, in general, more than compensates the decrease in the predicted X-ray luminosity from the scattering of the CMB photons.

A decrease in the predicted X-ray luminosities is expected if the relativistic particles are progressively depleted within the quasar radiation cones. With reference to Fig.1, which illustrates the application of our model to one of the sources discussed in the next section, one sees that by emptying the first 5–10 Kpc the expected luminosity would decrease by 10–20 %.

### 3. Results

We have applied our model to six high redshift, very powerful FRII radio galaxies which have been previously detected with ROSAT (3C 277.2, 280, 294, 324, 356 and 368). The IC computations have been made under the assumption of three different orientations of the radio axis with respect to the line of sight, that is 90, 60 and 45 degrees. For each configuration we have derived the luminosity of the hidden quasar which is required to match the observed total soft X-ray luminosity of each source and the ratio between the X-ray fluxes of the two lobes predicted by our model. The source fluxes at 178 MHz and the radio spectra have been taken from Laing et al. (1983) and Herbig et al. (1992). The extension and shape of the ellipsoidal distribution of the relativistic particles for each radio galaxy have been inferred from the available radio-maps. A detailed discussion for each object is reported in the following, while the main results are summarized in Table 1.

#### 3.1. 3C 277.2 ( $z=0.776$ )

This radio galaxy has been observed with ROSAT PSPC for a total exposure time of 13.5 ksec and detected only at the  $3\sigma$  level, corresponding to about 12 source net counts (Crawford & Fabian 1995). Assuming the X-ray spectrum predicted by our IC model, a power law of energy index 0.95, the derived 0.2–4.0 keV luminosity is  $2.6 \times 10^{43}$  erg s $^{-1}$ . The overall angular extension of the radio structure is  $\sim 58$  arcsec and the radio volume has been modeled (ellipsoid semi-axis 192  $\times$  35 Kpc) by making use of the 1502 MHz map from Pedelty et al. (1989). If 3C 277.2 lies on the sky plane ( $\theta_{ax} = 90^\circ$ ), we find that the IC scattering of the CMB photons may contribute up to 22% of the source X-ray flux, while the required luminosity of a hidden quasar which could account for the remaining part of the observed flux via the IC process would be  $0.93 L_{\langle Q \rangle}$ . The predicted total angular size of the X-ray source is  $\sim 20$  arcsec for an e-folding drop in the luminosity profile.

If the radio axis inclination is  $\theta_{ax} = 60^\circ$  the corresponding figures would be 24% and  $0.80 L_{<Q>}$ , while the X-ray source would appear asymmetric with one lobe being  $\sim 3$  times brighter than the other one.

The presence of a hidden quasar in 3C 277.2 has already been proposed to explain the strong radio-optical alignment and the high degree of polarization of the optical spectrum (di Serego Alighieri 1994 and ref. therein). From a recent modeling based on dust scattering it is estimated that the hidden quasar would have a magnitude  $m_V \simeq 17.2$  (Manzini & di Serego Alighieri 1996). It is interesting to note that, by assuming the *typical* quasar spectrum, the V magnitude of the hidden quasar required by our model would be 16.9 and 17.1, for  $\theta_{ax} = 90^\circ$  and  $60^\circ$  respectively, in very good agreement with the above estimate.

### 3.2. 3C 280 ( $z=0.996$ )

3C 280 is one of the most powerful FRII radio galaxies. Deep optical imaging revealed that the  $[OII]$  emission lines of this radio galaxy are edge-brightened and lie along the boundaries of the radio lobes (McCarthy et al. 1995 and references therein). The source is quite faint in the soft X-ray energy band giving only about 71 net counts on a deep ROSAT PSPC exposure of about 48 ksec (Worrall et al. 1994). The spectrum is poorly constrained being consistent with a power law spectral index  $0.5 < \alpha < 2.0$  and an upper limit on the intrinsic absorption of  $4 \times 10^{21} \text{ cm}^{-2}$  suggesting that the soft X-ray emission is not intrinsically absorbed. By adopting a spectral index  $\alpha = 0.71$ , consistent with the radio data, we find a luminosity of  $6.9 \times 10^{43} \text{ erg s}^{-1}$  in the 0.2–4.0 keV energy band. Worrall et al. (1994) state that a combination of a point source and of an extended emission, described by a  $\beta$  model with core radius between  $18''$  and  $65''$ , provides a better fit to the X-ray data.

The angular size of the radio structure is 18 arcsec and we have modeled the radio volume (ellipsoid semi-axis  $62 \times 22 \text{ Kpc}$ ) with reference to the 1.4 GHz map of Ronghui et al. (1992). If 3C 280 lies on the plane of the sky, the IC contribution to the soft X-ray luminosity from the scattering of the CMB photons could be as high as 22% and the luminosity of a hidden quasar which would be required to IC produce the soft X-ray total luminosity would be about that of the *typical* quasar, i.e.  $L_{<Q>}$ . The total angular size along the radio axis of the X-ray source predicted by our model would be  $\sim 12$  arcsec for an e-folding drop in the luminosity profile (Fig.1). The ratio between the X-ray luminosities of the two lobes could range from 1 to 4 depending on the inclination of the radio axis with respect to the line of sight. On the other hand if, according to Worrall et al. (1994), it is assumed that the point-like source represents only 60% of the total luminosity and that the remaining 40% is due to cluster emission, then the required hidden quasar luminosity would be  $\sim 0.52 L_{<Q>}$ , while the IC contribution due to the CMB photons would increase to  $\sim 38\%$ . Our model may represent a straightforward interpretation of the X-ray properties of this radio galaxy.

### 3.3. 3C 294 ( $z=1.786$ )

3C 294 is a well known example of the optical/radio alignment (McCarthy et al. 1990, McCarthy 1993). The monochromatic luminosity of the detected  $\text{Ly}\alpha$  line is  $7.6 \times 10^{44} \text{ erg s}^{-1}$  and it shows large intrinsic widths ( $700$ – $2600 \text{ km s}^{-1}$ ). A possible interpretation of the observed properties has been suggested by McCarthy et al. (1990) assuming a powerful non-thermal central source with a luminosity comparable to that of a luminous quasar which ionizes the gas clouds. 3C 294 has been observed with ROSAT PSPC (Crawford & Fabian 1996b) for a total exposure time of 22.69 ksec. The signal is very faint giving only  $\sim 25$  source net counts. The observed flux is consistent with either a thermal spectrum or an unabsorbed power law. Assuming a power law spectrum with spectral index  $\alpha = 1.1$ , consistent with the radio one, a 0.2–4.0 keV rest frame luminosity of  $\sim 3.0 \times 10^{44} \text{ erg s}^{-1}$  is inferred.

The radio structure has been modeled (ellipsoid semi-axis  $95 \times 30 \text{ Kpc}$ ) by making use of 5 GHz map of Strom et al. (1990). It has an angular size of 20 arcsec. The contribution due to the IC scattering of the CMB photons is  $\sim 2.9 \times 10^{43} \text{ erg s}^{-1}$ , i.e.  $\sim 10\%$  of the soft X-ray luminosity. The luminosity of the hidden quasar required to match the total soft X-ray luminosity would be  $\sim 3.6$ – $4.5 L_{<Q>}$  depending on the inclination of the radio axis on the sky plane. This is a very luminous quasar, but we note that it may be consistent with the hypothetical radiation source required to explain the observed strength of the  $\text{Ly}\alpha$  emission line. The predicted ratio between the X-ray luminosities of the two lobes would be between 1 and 7 depending on the inclination of the radio galaxy on the sky plane. In the case of a unit ratio the total angular size of the X-ray source along the radio axis would be  $\sim 10$  arcsec.

### 3.4. 3C 324 ( $z=1.206$ )

This radio galaxy shows optical/radio alignment (McCarthy 1993) and a high degree of polarization ( $\sim 18\%$ ) in the R-band (di Serego Alighieri et al. 1993). From a recent modeling based on dust scattering of the nuclear light the V magnitude of the hidden quasar is estimated to be  $m_V \sim 18.5$  (Manzini & di Serego Alighieri 1996). 3C 324 has been observed with the ROSAT PSPC (Crawford & Fabian 1996b) for a total exposure time of 15.4 ksec. The spectral shape is ill defined being consistent with either a thermal spectrum or with a highly absorbed power law. Assuming the power law spectrum predicted by our model from the radio data ( $\alpha = 1.07$ ) we find a a rest-frame 0.2–

4.0 keV luminosity  $\sim 1.7 \times 10^{44}$  erg s $^{-1}$ , a rather luminous X-ray source.

The radio structure has been modeled (ellipsoid semi-axis  $58 \times 23$  Kpc) by making use of the 1400 MHz map from Fernini et al. (1993). Its extension subtends an angle of  $\sim 14$  arcsec. The IC contribution due to the scattering of the CMB photons is only  $\sim 4\%$  and it does not change significantly with the inclination of the radio axis with respect to the line of sight, while the luminosity of the hidden quasar which would be required to match the total soft X-ray luminosity is  $5.1\text{--}6.0 L_{\langle Q \rangle}$  depending on the inclination of the radio axis. If one assumes the *typical* quasar spectrum of our model, the inferred V magnitude would be 16.2–16.4 at variance with the estimate of Manzini & di Serego Alighieri reported above. It should be noted that recent HST observations suggest that 3C 324 lies in a cluster of galaxies (Crawford & Fabian 1996b and ref. therein) whose thermal emission may provide a more satisfactory explanation of this X-ray luminous source.

### 3.5. 3C 356 ( $z=1.086$ )

3C 356 has been observed with the ROSAT PSPC for 18.6 ksec and detected at the  $\sim 6\sigma$  level for a total of  $\sim 30$  net counts (Crawford & Fabian 1993). While the spectrum is well fitted by a hot thermal plasma model, it is inconsistent with an absorbed power law, Cygnus A type. It should be stressed, however, that an unabsorbed power law with spectral index  $\sim 1.0$ , such as that predicted by our IC model, gives an adequate representation of the data. By adopting this spectral slope one derives a luminosity  $\sim 1.4 \times 10^{44}$  erg s $^{-1}$  in the 0.2–4.0 keV energy interval. From the analysis of the PSPC data it has been suggested that the source is extended, a good description being that of a point-like source (with radius  $r < 12''$ ) contributing  $\sim 20\%$  of the flux and an extended component approximately aligned with the radio axis. This has been confirmed by a subsequent observation with the ROSAT HRI, which failed to detect a point source at the position of the radio galaxy at the flux level expected from the PSPC observation (Crawford & Fabian 1996a). These authors suggest that the most likely interpretation of the source is that of the emission from a hot intracluster gas in a cluster of galaxies hosting 3C 356.

The radio structure (ellipsoid semi-axis  $290 \times 70$  Kpc) has been derived from the 1490 MHz map of Leahy et al. (1989). The angular size subtended by the hot spots is  $\sim 80$  arcsec. Since 3C 356 is the radio galaxy with the largest volume in our sample, the IC contribution from the scattering of the CMB photons is expected to be important. Assuming that the radio galaxy lies on the plane of the sky, we find that this contribution accounts for  $\sim 37\%$  of the soft X-ray luminosity. The inferred hidden quasar luminosity, which would be required to account for the remaining soft X-ray luminosity of the source, is  $\sim 3.7 L_{\langle Q \rangle}$ . The predicted angular size of the source along the

radio axis would be  $\sim 36$  arcsec for an e-folding drop in the radial luminosity profile. If the inclination of the radio axis with respect to the line of sight is substantial, say  $\theta_{ax} = 60^\circ$ , the efficiency of the IC model increases and we expect an asymmetric source with a luminosity ratio  $\sim 3$  between the two X-ray lobes.

New optical spectropolarimetric data (Cimatti et al. 1997) obtained with the Keck Telescope show that the two radio-optical components (a & b) are polarized in the UV rest frame continuum emission and that there is a broad MgII $\lambda 2800$  emission line both in total and polarized light associated with component (a), indicating that 80% of the  $2800\text{\AA}$  flux is contributed by non-stellar radiation. These authors conclude that their observations definitely support the AGN unification model, but that it remains unclear which of the two components is hosting the hidden quasar: if it is located in component (b), then its luminosity would have to be at least as high as the maximum luminosity observed in 3C quasars, while if located in component (a) the energy requirements would be greatly alleviated leading to a luminosity closer to that of a *typical* quasar. The luminosity of the hidden quasar required by our model is consistent with these findings.

### 3.6. 3C 368 ( $z=1.132$ )

This is one of the best studied  $z \sim 1$  radio galaxies. It shows an imponent emission region oriented along the radio axis (Chambers et al. 1988). Several models have been proposed to interpret the emission lines and their complex velocity structure and the elongated continuum morphology. Djorgovski et al. (1987) suggest an interpretation in terms of a violent star burst caused by a merger between galaxies, while Meisenheimer & Hipplelein (1992) suggest that both the emission lines luminosity and their spatial and kinematic structure can be explained by the interaction between the radio jets and a high density ( $n_e \sim 0.1$  cm $^{-3}$ ) surrounding medium. However, both these models could not account for the detection of extended strong optical polarization, a *prima facie* evidence of scattered light from a hidden, luminous quasar (Cimatti et al. 1993 and ref. therein). More recent investigations, although not inconsistent with the possible existence of a hidden quasar, failed detecting any polarized component (upper limits of 2–3%) in 3C 368, while at the same time they lend further support to the idea that the strong emission associated with the aligned material is due to the interaction with the radio jets (Stockton et al. 1996 and ref. therein). 3C 368 has been observed with the ROSAT PSPC (Crawford & Fabian 1995) for a total exposure time of 26.4 ksec. It was detected at the  $\sim 5\sigma$  level giving only  $\sim 20$  source net counts. Assuming a power law spectrum with  $\alpha = 1.1$ , consistent with the radio spectral index, we find that the 0.2–4.0 keV rest frame luminosity is  $\sim 1.5 \times 10^{44}$  erg s $^{-1}$ .

The model radio structure (ellipsoid semi-axis  $54 \times 18$  Kpc) has been derived from the 5 GHz map of Chambers

**Table 1.** The soft X-ray luminosity and source angular sizes of six powerful FRII radio galaxies from the IC scattering of hidden quasar and CMB photons.

(1) Name	(2) z	(3) $\theta_{ax}$	(4) $B_{eq}$ ( $10^{-5}$ G)	(5) $L_X(<Q>)$ ( $10^{43}$ erg s $^{-1}$ )	(6) $L_X(CMB)$ ( $10^{43}$ erg s $^{-1}$ )	(7) $L_Q/L_{<Q>}$	(8) $l$	(9) e-fold (arcsec)
3C 277.2	0.766	90°	3.17	2.28	0.56	0.93	1	10
		60°	3.04	2.42	0.61	0.80	3.1	
		45°	2.92	2.64	0.66	0.76	4.4	
3C 280	0.996	90°	4.65	5.15	1.42	1.08	1	6
		60°	4.47	5.48	1.53	0.99	2.8	
		45°	4.24	5.61	1.67	0.94	3.8	
3C 294	1.786	90°	10.03	6.12	2.98	4.56	1	5
		60°	9.66	6.89	3.22	4.01	4.2	
		45°	9.23	7.44	3.54	3.68	7.1	
3C 324	1.206	90°	9.37	4.73	1.12	6.10	1	3
		60°	8.90	5.23	1.21	5.50	4.4	
		45°	8.38	5.50	1.31	5.21	8.6	
3C 356	1.086	90°	2.56	2.88	3.90	3.70	1	18
		60°	2.43	3.15	4.21	3.25	2.8	
		45°	2.29	3.32	4.61	2.97	3.6	
3C 368	1.132	90°	9.71	8.01	0.54	1.85	1	4
		60°	9.42	9.02	0.57	1.64	4.9	
		45°	8.80	9.84	0.66	1.49	10.0	

**Col.1** Source name; **Col.2** Redshift; **Col.3** Angle between the radio-axis and the line of sight; **Col.4** Values of the equipartition magnetic field in the lobes (Eq.A3); **Col.5** The IC X-ray luminosity in the 0.2–4.0 keV band (source frame) assuming a *typical* hidden quasar; **Col.6** The IC X-ray luminosity in the 0.2–4.0 keV band (source frame) from the scattering of the CMB photons; **Col.7** The required luminosity of the hidden quasar (in unit of a *typical* quasar) to match the observed X-ray luminosity; **Col.8** The predicted X-ray ratio between the two lobes; **Col.9** The predicted angular size (radius) for an e-folding drop in the luminosity profile.

et al. (1988). The radio source is rather small, subtending an angle of only 14 arcsec, which means that the associated rather strong equipartition field prevents any major contribution ( $\sim 4\%$ ) from the IC scattering of CMB photons. The required luminosity of the hidden quasar to IC produce the observed soft X-ray luminosity is  $\sim 1.5$ – $1.9 L_{<Q>}$ , depending on the inclination of the radio axis. The predicted angular size of the X-ray source would be  $\sim 4$  arcsec. Assuming an inclination of the radio axis  $\theta_{ax} = 60^\circ$ , the required hidden quasar luminosity would be  $\sim 1.6 L_{<Q>}$  and the luminosity ratio between the two X-ray lobes  $\sim 5$ . We conclude that the soft X-ray luminosity of 3C 368 may be entirely accounted for by our model.

### 3.7. The case of Cygnus A

One may wonder whether our model could be tested in the case of the (close by) archetypal FRII radio galaxy Cygnus A. Assuming the presence of a *typical* quasar in the nucleus of Cygnus A, we find an IC luminosity in the 0.2–4.0 keV band  $\sim 2 \times 10^{43}$  erg s $^{-1}$ , which is  $\sim 50$ – $100$  times lower than the thermal emission of the surrounding hot intracluster gas. Furthermore, the predicted e-folding drop in the luminosity profile corresponds to an angular

size ( $\sim 30$  arcsec) of the same order as that of the cluster emission.

Even assuming that the brightness distribution predicted by our model (roughly  $\propto 1/r$ ) could be extrapolated well inside the central region, its value would still be small (at most 10–15 %) compared to that of the cluster emission. One can conclude that the soft X-ray luminosity predicted by our model, although of similar strength as those derived for the high redshift powerful FRII radio galaxies, is shadowed by the presence of the strong cluster emission. ROSAT HRI observations of the central part of Cygnus A have revealed a point-like source, identified with the unabsorbed quasar emission, and the possible presence of a weak extended emission ( $\sim 10$  arcsec; Harris et al. 1994b) in addition to that of the cluster gas. If confirmed, such extended emission could be consistent with our model.

## 4. Summary and Conclusions

We have shown that, in the framework of the unification scheme relating quasars and FRII radio galaxies, the contribution to the soft X-ray emission of strong radio galaxies via the IC scattering of the optical-IR photons from a hidden quasar may be important. Given a *typical* quasar

spectrum, the main contribution comes from the IC scattering of the IR photons under the assumption that the spectrum of the radio emitting electrons can be extrapolated down to lower energies ( $\gamma \sim 100 - 200$ ). For all sources discussed in this work our estimates of the particles and fields energy densities are derived from minimum energy condition by imposing the same low energy cut off ( $\gamma_{min} = 20$ ) in the particle distribution. There is no direct observational evidence of how far one can extrapolate the radio electron spectrum to lower energies. The assumption  $\gamma_{min} = 20$  appears consistent with present knowledge of the physical conditions prevailing in the radio sources. If we had chosen a larger  $\gamma_{min}$ , but less than  $\sim 100$ , then we would have obtained larger normalizations of the electron spectra and larger predicted soft X-ray luminosities. This statement holds even taking into account the fact that the contribution from the IC scattering of the optical–near IR photons emitted by a hidden quasar would progressively tend to zero. In this case, however, the predicted soft X-ray spectrum would be significantly flatter.

Given the directionality of the photon flux propagating outward from a hidden quasar, the standard formulae for the computation of the IC emission are not applicable. We have derived the general formulae for the anisotropic IC scattering in the Thompson approximation and discussed them in the Appendix B together with those specifically applied to our model.

The observed soft X-ray properties of six strong FRII radio galaxies have been compared with those predicted by our model. Such objects are some of the stronger high redshift FRII radio galaxies in the 3CR sample for which X-ray data are available at the moment. Our estimates include the contributions to the soft X-ray fluxes due to the IC scattering of the radio electrons with the CMB photons which, because of the high redshifts involved, may be significant. In our computations we have assumed that the radio volumes can be approximated by prolate ellipsoids filled with a uniform distribution of particles and fields and that the energy density of the relativistic electrons equals that of the protons. These volumes may be significantly larger than those filled by the relativistic particles, but in Sect. 2.3 we have shown that this may lead to larger predicted values only for the fraction (generally small) of the total X-ray luminosity from the IC of the CMB photons.

We find that for three radio galaxies (3C 277.2, 3C 280 and 3C 368) the model predicted soft X-ray luminosities agree with those observed if a quasar of average strength is supposed to be hidden in their nuclei. It is interesting to note that in the case of 3C 277.2 the derived optical luminosity of the hidden quasar is in very good agreement with that inferred from spectropolarimetric studies. The predicted soft X-ray spectrum of 3C 280 is compatible with that observed and with the evidence of a low  $N_H$  column density. For the remaining three radio galaxies of our sample (3C 294, 3C 324 and 3C 356) we find that

the hidden quasars must be significantly more powerful than the *typical* quasar in order to match the observed soft X-ray luminosities. In the case of 3C 294 the hidden quasar would have to be  $\sim 1.5$  magnitude more luminous than the *typical* quasar, which may be consistent with the very strong Ly $\alpha$  emission observed in this radio galaxy. A similarly powerful hidden quasar is required for 3C 356, in which case our model may provide a possible interpretation of both the extension and alignment with the radio structure of the soft X-ray source and of its (poorly constrained) spectral shape. The presence of a luminous hidden quasar is strongly supported by recent spectropolarimetric studies of this source. In the case of 3C 324 the required optical-IR luminosity of the hidden quasar is about 2 magnitudes brighter than that of the *typical* quasar and considerably higher than that inferred from spectropolarimetric studies, but recent HST observations suggest that 3C 324 may lie in a cluster of galaxies whose thermal emission is likely to dominate the X-ray flux detected in the direction of this radio galaxy. In addition, we have briefly discussed the special case of Cygnus A showing that the soft X-ray luminosity predicted by our model is completely dwarfed by the very strong emission of the surrounding hot intracluster gas. Thanks to the solution of the anisotropic IC equations, for each radio galaxy we are able to compute the expected ratio between the X-ray luminosities of the lobes as a function of the inclination of the radio axis on the sky plane and of the differential electrons spectrum. This ratio may be large and it can provide a direct observational handle on the applicability of our model. If detected, this effect could also tell us which of the two lobes is the farthest. Unfortunately our model forecasts an extended X-ray emission with a somewhat steep brightness profile (roughly  $\propto 1/r$ ) so that the small ( $< 20$  arc sec) angular size of the distant strong FRII radio galaxies and their relatively weak X-ray emission make these observational tests difficult to be performed with present X-ray facilities. The expected X-ray luminosity profile (Fig. 1) shows that a depletion of the relativistic particles in the mid–central source volume may significantly decrease the efficiency of our model. Under the conservative assumption whereby the relativistic electrons are only present within the radio lobes defined by the high frequency radio maps, we find that the estimates of the X-ray luminosities of Table 1 are reduced by factors from 2 to 3.

Clearly the predictions of our model are based on various assumptions concerning the physical properties of the FRII radio galaxies. We believe to have shown that reasonable choices of the parameters lead to results that can be tested with observations. In particular, the imaging and spectral capabilities of the future X-ray facilities, such as AXAF, may provide a unique tool to study the distribution and spectra of the relativistic electrons at lower energies thus bringing an important information on the structure and evolution of these sources.

*Acknowledgements.* The authors would like to thank A. Cimatti, S. di Serego Alighieri, A.C. Fabian, R. Fanti and G. Ghisellini for useful discussions and informations and the anonymous referee whose constructive criticism and suggestions have considerably improved the presentation of this work. AC acknowledges partial financial support from the Italian Space Agency under the contract ASI-95-RS-152. This research has made use of the NASA/IPAC Extragalactic Database (NED) which is operated by the Jet Propulsion Laboratory, Caltech, under contract with the National Aeronautics and Space Administration.

### A. Equipartition equations

In this Appendix we derive equipartition quantities based on a low energy cut-off in the particle energy distribution, instead of a low frequency cut-off in the emitted synchrotron spectrum. Under the assumption that the differential energy distribution of the relativistic electrons is represented by a single power law,  $N(\gamma) = K_e \gamma^{-\delta}$ , the total (particles and fields) energy density can be written as:

$$w_{tot} = \frac{B^2}{8\pi} + (1+F) mc^2 \int_{\gamma_{min}}^{\gamma_{max}} K_e \gamma^{-\delta+1} d\gamma \quad (A1)$$

where  $F$  is the ratio between the energy densities of the relativistic proton and electron components and  $m$  is the electron mass. From the standard synchrotron theory  $K_e = j(\nu) a(\delta) B^{-\frac{\delta+1}{2}} \nu^{\frac{\delta-1}{2}}$ , where  $j(\nu)$  is the synchrotron emissivity at a frequency  $\nu$  and  $a(\delta)$  a constant. Assuming  $\delta > 2$  and  $\gamma_{max} \gg \gamma_{min}$ , Eq.(A1) becomes:

$$w_{tot} = \frac{B^2}{8\pi} + \frac{(1+F)a(\delta)\nu^{\frac{\delta-1}{2}} mc^2}{\delta-2} B^{-\frac{\delta+1}{2}} j(\nu) \gamma_{min}^{2-\delta} \quad (A2)$$

By imposing the minimum energy condition, under the assumption that the particle and magnetic field energy densities are uniformly distributed in a volume  $V$ , and that particle momenta and field lines are randomly distributed, one finds the equipartition magnetic field strength

$$B_{eq} = \left[ C(\delta) \frac{P(\nu)}{V} \nu^{\frac{\delta-1}{2}} (1+F) \right]^{\frac{2}{\delta+5}} \gamma_{min}^{\frac{2(2-\delta)}{(\delta+5)}} \quad (A3)$$

with

$$C(\delta) = \frac{\Gamma(\frac{\delta}{4} + \frac{7}{4})}{\Gamma(\frac{\delta}{4} + \frac{19}{2}) \Gamma(\frac{\delta}{4} - \frac{1}{12}) \Gamma(\frac{\delta}{4} + \frac{5}{4})} \left( \frac{2\pi mc}{3e} \right)^{\frac{\delta-1}{2}} \cdot 4\sqrt{\pi/3} e^{-3} (mc^2)^2 (\delta+1)^2 (\delta-2)^{-1} .$$

where  $P(\nu)$  is the source synchrotron power at a frequency  $\nu$ ,  $\Gamma$  is the Euler function, and  $e$  the (positive) electron charge. Representative values of  $C(\delta)$  are given in Table 2. It should be noticed that, at variance with the classical equipartition equations, here the energy density

of the relativistic particles is exactly equal to that of the magnetic field (instead of  $4/3$ ).

It may be helpful for practical applications to write down the relationship between our equipartition quantities and those (primed) derived from the standard equipartition equations with reference to the observed radio flux densities in the 10 MHz – 100 GHz frequency band (source frame). We find:

$$B_{eq} = D(\delta) \gamma_{min}^{\frac{2(2-\delta)}{\delta+5}} (B'_{eq})^{\frac{7}{\delta+5}} \quad (A4)$$

where  $D(\delta)$  is  $\sim 1$  (Table 2). It should be noticed that  $B_{eq} > B'_{eq}$  for  $B'_{eq} < D(\delta) \gamma_{min}^{-2}$ , in which case  $K_e < K'_e$  follows from the synchrotron emissivity formulae (i.e.  $K_e B_{eq}^{(\delta+1)/2} = K'_e (B'_{eq})^{(\delta+1)/2}$ ).

**Table 2.** Numerical values of  $C(\delta)$  and  $D(\delta)$  for some values of  $\delta$

$\delta$	$C(\delta)$	$D(\delta)$
2.3	1.70 E8	1.00
2.5	2.50 E7	1.01
2.7	4.37 E6	1.05
2.9	8.05 E5	1.09
3.1	1.55 E5	1.14
3.3	3.06 E4	1.17

### B. Anisotropic inverse Compton scattering

In this Appendix we derive the basic formulae for the computation of the X-ray emission predicted by our model as a result of the IC scattering of the photons from a hidden quasar with the relativistic electrons in the radio lobes. We note that such a calculation can not be performed with the standard IC equations usually found in the literature (Jones 1968; Blumenthal & Gould 1970) essentially for two main reasons: first, in our quasar model the relativistic electrons are flooded by an anisotropic photon flux and, second, the ultra-relativistic limit ( $\beta = 1$ ) may not be completely applicable. The computation has been performed in three successive steps. First of all the IC spectrum resulting from the interaction between an unidirectional photon beam and an electron of energy  $mc^2\gamma$  has been derived. Then the IC emissivity due to the interaction between an unidirectional photon beam and a population of relativistic electrons with a power-law energy distribution and an isotropic distribution of their momenta has been computed. The anisotropic emission is described as a function of the angle between the photon beam and the line of sight. Finally the total IC emission toward the observer is obtained by integrating the emissivity over the radio lobe volume for a given inclination of

the radio galaxy on the sky plane and for a given angular distribution of the radiation from the hidden quasar. All the calculations have been performed in the Thompson limit.

### B.1. Scattering of a photon beam by a single electron.

First of all we define the geometry of the scattering process by assuming that the motion of the incident photons is along the z-axis (**Fig. 2**).

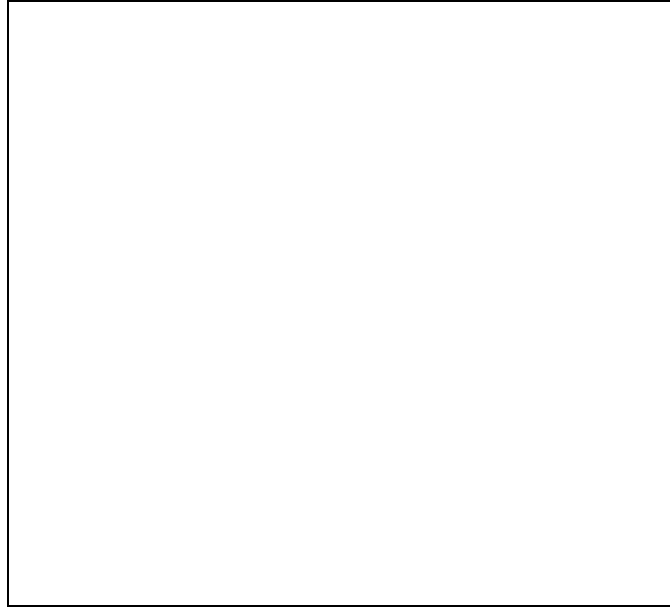


**Fig. 2.** The geometry of the scattering between one electron with momentum in the  $(\theta, \phi)$  direction and a photon beam propagating along the z-axis. The scattered photon direction is indicated by the  $(\theta_{SC}, \phi_{SC})$  coordinates.

The momenta of the incident and scattered photons (of energy  $\epsilon$  and  $\epsilon_1$ ) and of the electron are respectively described by the four-vectors:

$$P = \frac{\epsilon}{c} (1, 0, 0, 1) \quad (B1)$$

$$P_1 = \frac{\epsilon_1}{c} (1, k_1, k_2, k_3) \quad (B2)$$

$$P_e = mc\gamma (1, \beta e_1, \beta e_2, \beta e_3) \quad (B3)$$

where  $k_j$  and  $e_j$  represent the unit vector components in a spherical coordinate system and  $\beta \equiv v/c$ .

Let us consider a monochromatic unidirectional photon beam (of energy  $\epsilon_i$ ) so that the photon number density seen by an electron per unit solid angle and energy is

$$n(\epsilon, x, \phi) d\epsilon dx d\phi = n \delta(\epsilon - \epsilon_i) \delta(x - x_i) \delta(\phi - \phi_i) d\epsilon dx d\phi \quad (B4)$$

where  $\theta$  and  $\phi$  are the angles that describe the electron momentum in spherical coordinates,  $x = \cos \theta$  and  $\delta$  is the  $\delta$ -function.

The ratio  $dn/\epsilon$  is known to be a relativistic invariant (e.g. Blumenthal & Gould 1970), so that from (B4) the total differential photon density in the electron frame (primed) is:

$$\frac{dn'(\epsilon', \Omega'; \epsilon, \Omega)}{d\epsilon' d\Omega'} = n \delta(\epsilon - \epsilon_i) \frac{d\Omega d\epsilon}{d\Omega' d\epsilon'} \frac{\epsilon'}{\epsilon} \delta(x - x_i) \delta(\phi - \phi_i) \quad (B5)$$

The angular and energy distribution of the scattered photons per unit time in the electron frame is:

$$\frac{dN_{\gamma, \epsilon}}{dt' d\epsilon' d\Omega'_{SC} d\Omega' d\epsilon'_1} = \frac{dn'(\epsilon', \Omega'; \epsilon, \Omega)}{d\epsilon' d\Omega'} \frac{c d\sigma}{d\Omega'_{SC} d\epsilon'_1} \quad (B6)$$

where  $N$  = the total number of scatterings (invariant),  $c$  is the light velocity and

$$\frac{d\sigma}{d\Omega'_{SC} d\epsilon'_1} = \frac{r_0^2}{2} (1 + \cos^2 \theta'_{SC}) \delta(\epsilon'_1 - \epsilon') \quad (B7)$$

is the differential Thompson cross section,  $\theta'_{SC}$  being the angle between the incident and scattered photon in the electron frame,  $d\Omega'_{SC} = -d(\cos \theta'_{SC}) d\phi'_{SC}$  and  $r_0$  the classical electron radius.

The energy distribution of the scattered photons in the electron frame is thus:

$$\frac{dN_{\gamma, \epsilon}}{dt' d\Omega'_{SC} d\epsilon'_1} = \frac{r_0^2 c}{2} \int \int_{(\epsilon', \Omega')} \frac{dn'(\epsilon', \Omega'; \epsilon, \Omega)}{d\epsilon' d\Omega'} \cdot (1 + \cos^2 \theta'_{SC}) \delta(\epsilon'_1 - \epsilon') d\epsilon' d\Omega' \quad (B8)$$

From a Lorentz boost of Eqs.(B1),(B2),(B3) one obtains:

$$\cos \theta'_{SC} = 1 + \frac{(k_3 - 1)}{\gamma^2 L L_1} \quad (B9)$$

and

$$\cos(\phi'_{SC} - \phi_0) = \{\cos \theta'_{SC} L_1 \Delta - L((\gamma - 1)e_j k_j e_3 + k_3 - \gamma \beta e_3)\} \left[ (1 - \cos^2 \theta'_{SC}) \left(1 - (\Delta/L)^2\right) L L_1 \right]^{-1} \quad (B10)$$

where  $L = (1 - \beta e_3)$ ,  $L_1 = (1 - \beta e_j k_j)$ ,  $\Delta = (\gamma - 1)e_3^2 + 1 - \gamma \beta e_3$  and  $\phi_0$  an arbitrary phase. The Jacobian of  $\Omega'_{SC}$  with respect to  $\Omega_{SC}$  is:

$$\frac{d\Omega'_{SC}}{d\Omega_{SC}} = \frac{1}{\gamma^2 L_1^2} \quad (B11)$$

Finally, the emitted power spectrum per unit frequency and solid angle in the lab frame is obtained by considering the relativistic transformation  $\gamma dt' = dt$ ,  $d\epsilon'_1 = \gamma(1 - \beta e_j k_j)d\epsilon_1$ ,  $\epsilon' = \gamma\epsilon(1 - \beta e_3)$  and Eqs. (B5), (B8), (B9), (B11). We obtain:

where

$$\frac{dE(P_e, P, P_1)}{dtd\epsilon_1 d\Omega_{SC}} = \frac{cr_0^2}{2\gamma^2} n \frac{\epsilon_1}{L_1} \delta(\epsilon - \epsilon_i) \left[ \left( \frac{(k_3 - 1)}{\gamma^2 LL_1} \right)^2 + 2 + 2 \frac{(k_3 - 1)}{\gamma^2 LL_1} \right] \quad (\text{B12})$$

together with the additional equation (with  $\epsilon_1 > \epsilon$ )

$$e_j k_j = \frac{1}{\beta} \left[ 1 - \frac{\epsilon}{\epsilon_1} L \right] \quad (\text{B13})$$

## B.2. Scattering of a photon beam by electrons with isotropic momenta distribution

The emitted power per unit frequency and solid angle is obtained by integrating Eq.(B12) over  $\gamma$ ,  $e_3$ , and  $\phi$  assuming an isotropic distribution of the electrons momenta and a power law energy differential spectrum  $N_e(\gamma) = \frac{1}{4\pi} K_e \gamma^{-\delta}$

$$\frac{dW(\epsilon, P_1)}{dtd\epsilon_1 d\Omega_{SC}} = \frac{cr_0^2 K_e}{8\pi} n \int \int \int \gamma^{-(\delta+2)} \epsilon_1^2 \delta(\epsilon - \epsilon_i) \cdot \frac{1}{L\epsilon} \left[ 2 + \left( \frac{(k_3 - 1)}{\gamma^2 L^2} \frac{\epsilon_1}{\epsilon} \right)^2 + 2 \frac{(k_3 - 1)}{\gamma^2 L^2} \frac{\epsilon_1}{\epsilon} \right] de_3 d\phi d\gamma \quad (\text{B14})$$

From Eq.(B13) and the  $\delta$ -function properties we find:

$$\begin{aligned} \delta(\epsilon - \epsilon_i) &= \delta(\gamma - \tilde{\gamma}) \gamma^3 \beta \epsilon_1 \frac{(e_3 - e_j k_j)}{(\epsilon_1 e_j k_j - \epsilon e_3)^2} = \\ &= \delta(\gamma - \tilde{\gamma}) \frac{\gamma^3 \beta}{\epsilon_1} \frac{L^2}{[e_3 (1 - k_3) - e_1 k_1 - e_2 k_2]} \end{aligned} \quad (\text{B15})$$

where

$$\tilde{\gamma} = \left[ 1 - \left( \frac{\epsilon_1 - \epsilon_i}{\epsilon_1 e_j k_j - \epsilon e_3} \right)^2 \right]^{-\frac{1}{2}} = \left[ 1 - \tilde{\beta}^2 \right]^{-1/2} \quad (\text{B16})$$

is the Lorentz factor of the electrons for a particular scattering configuration, i.e. having fixed  $\epsilon_1$ ,  $e_3$  and  $e_j k_j$  for a given  $\epsilon_i$ , with the condition  $\beta e_j k_j \neq 1$ .

Due to the particular choice of the geometry, the problem is symmetric with respect to the z-axis. For this reason we may assume that the line of sight lies on the y-z plane and as a result, one has  $k_2 = 0$  and  $k_1 = \sqrt{1 - k_3^2}$ . From Eqs.(B15) and (B16), by renaming  $\epsilon_i$  with  $\epsilon$  and because  $\epsilon_1 = \sin \phi \sqrt{1 - e_3^2}$ , we can then integrate Eq.(B14) over the energy of the electrons to find

$$\begin{aligned} \frac{dW(\epsilon, k_3)}{dtd\epsilon_1 d\Omega_{SC}} &= \frac{cr_0^2 K_e n}{8\pi} \frac{\epsilon_1^2 (\epsilon_1 - \epsilon)}{\epsilon} \int \int a(e_3, \phi) \cdot \\ &\quad \left[ 2 + \left( \frac{(k_3 - 1)}{b(e_3, \phi)} \right)^2 + 2 \frac{(k_3 - 1)}{b(e_3, \phi)} \right] de_3 d\phi \end{aligned} \quad (\text{B17})$$

$$\begin{aligned} a(e_3, \phi) &= \{ -(\epsilon_1 - \epsilon)^2 + \\ &\quad [\epsilon_1 (\sin \phi \sqrt{1 - e_3^2} \sqrt{1 - k_3^2} + e_3 k_3) - e_3 \epsilon]^2 \}^{\frac{\delta-1}{2}} \cdot \\ &\quad \left( \epsilon_1 (\sin \phi \sqrt{1 - e_3^2} \sqrt{1 - k_3^2} + e_3 k_3) - e_3 \epsilon \right)^{-(\delta+1)} \end{aligned} \quad (\text{B18})$$

and

$$\begin{aligned} b(e_3, \phi) &= \epsilon_1 \epsilon \left[ \sin \phi \sqrt{1 - e_3^2} \sqrt{1 - k_3^2} + e_3 (k_3 - 1) \right]^2 \cdot \\ &\quad \{ \left[ \epsilon_1 (\sin \phi \sqrt{1 - e_3^2} \sqrt{1 - k_3^2} + e_3 k_3) - e_3 \epsilon \right]^2 \\ &\quad - (\epsilon_1 - \epsilon)^2 \}^{-1} \end{aligned} \quad (\text{B19})$$

Since Eq.(B17) cannot be integrated analytically, except for particular values of the parameters, we have performed a numerical integration over all possible scattering configurations. The limits of integration are obtained by requiring that  $0 < \tilde{\beta} \leq 1$ . The extremes of integration of  $e_3$  are derived from Eq.(B16) by setting  $\tilde{\beta} = 1$ :

$$\begin{aligned} e_3(\pm) &= (1 - \cos^2 \phi)^{\frac{1}{2}} \left[ \frac{(1 - \epsilon/\epsilon_1)(k_3 - \epsilon/\epsilon_1)}{(1 - k_3^2)^{\frac{1}{2}}(1 - \cos^2 \phi)^{\frac{1}{2}}} \pm \right. \\ &\quad \left. \left( (1 - k_3^2) \sin^2 \phi + (k_3 - \frac{\epsilon}{\epsilon_1})^2 - (1 - \frac{\epsilon}{\epsilon_1})^2 \right)^{\frac{1}{2}} \right] \cdot \\ &\quad (1 - k_3^2)^{\frac{1}{2}} \{ (1 - k_3^2) \sin^2 \phi + (k_3 - \frac{\epsilon}{\epsilon_1})^2 \}^{-1} \end{aligned} \quad (\text{B20})$$

The coincidence  $e_3(-) = e_3(+)$  is obtained for a  $\phi^*$  such that

$$\sin \phi^* = \left( 1 - \frac{2\epsilon}{\epsilon_1(1 + k_3)} \right)^{1/2}$$

Then the scattering domains can be described as follows: for a line of sight such that  $k_3 > -1 + 2\epsilon/\epsilon_1$  (but  $k_3 \neq 1$ ), then  $\phi^* < \phi < \pi - \phi^*$  and  $e_3(-) < e_3 < e_3(+)$ ; while for a line of sight such that  $k_3 \leq -1 + 2\epsilon/\epsilon_1$ , one has either  $0 \leq \phi < \pi$  and  $-1 < e_3 < e_3(+)$  or  $\pi \leq \phi \leq 2\pi$  and  $-1 < e_3 < e_3(-)$ .

The (normalized) emitted power per unit frequency and solid angle is shown in **Fig.3** for three values of  $\delta$  as a function of  $\theta_{SC}$ .

It should be noted that the spectral slope depends on both the ratio  $\epsilon_1/\epsilon$  and  $k_3$ . This is due to the varying geometry of the scatterings and to the fact that we have relaxed the ultra-relativistic ( $\beta = 1$ ) approximation. For example, assuming an energy of the incident photons  $\epsilon = 0.1$  eV and  $\delta = 2.5$ , we find that the spectral index between 10 and 20 eV is 0.727, 0.737 and 0.754 respectively for  $\theta_{SC} = 3.12, 2.20$  and 1.50. However, these differences

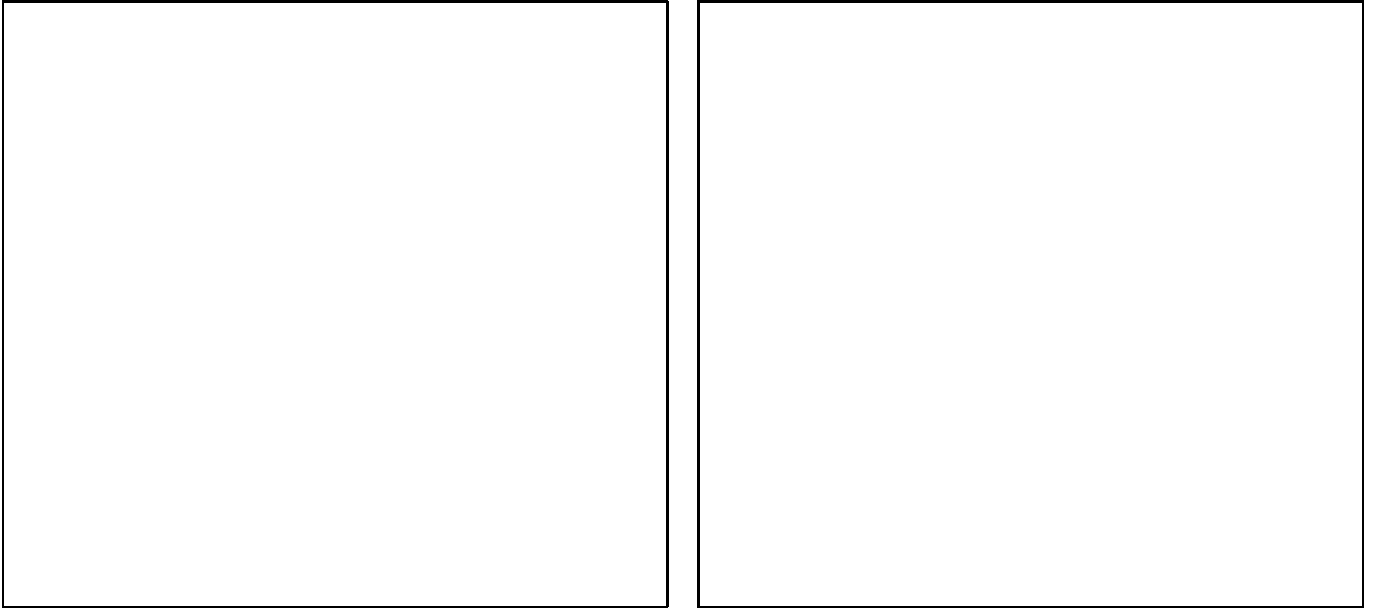


**Fig. 3.** The normalized IC emitted power per unit frequency and solid angle as a function of the scattering angle is plotted for three representative values of the electrons spectral index  $\delta$ : 3.0 (solid line), 2.5 (dotted line) and 2.0 (dashed line).

vanish at somewhat higher energies, as it should be: for photon energies larger than  $\epsilon_1 = 2$  keV we recover the classical  $\alpha = 0.750$  for all the  $\theta_{SC}$  (a more detailed discussion will be given elsewhere). From the standpoint of the model discussion presented in this paper these differences can be neglected.

### B.3. Application of the IC formulae to our source model

Here the photon number depends on the distance  $r$  from the hidden quasar and it can be easily computed for a band (of lower and upper energy  $\epsilon_L, \epsilon_U$ ) of the quasar spectrum. If  $L_{Q,b}$  is the quasar luminosity in such band and  $d$  the spectral index, the photon number per unit volume and unit energy interval is

$$n(\epsilon, r) = \frac{(d-1)\epsilon^{-(d+1)}}{4\pi c r^2 [\epsilon_L^{-(d-1)} - \epsilon_U^{-(d-1)}]} L_{Q,b} \quad (\text{B21})$$

From Eqs.(B17) and (B21) one can write:

$$\frac{dW(r, k_3)}{dt d\epsilon_1 d\Omega_{SC}} = \frac{r_0^2 K_e (d-1) \epsilon_1^2}{32\pi^2 [\epsilon_L^{-(d-1)} - \epsilon_U^{-(d-1)}]} r^{-2} L_{Q,b} \cdot \int I(\epsilon_1, k_3; \epsilon, e_3, \phi) \epsilon^{-(d+2)} d\epsilon \quad (\text{B22})$$

where  $I(\epsilon_1, k_3; \epsilon, e_3, \phi)$  is the integral in Eq.(B17) with  $n = n(\epsilon) d\epsilon$ .

**Fig. 4.** The ellipsoidal distribution of the relativistic particles, for a given inclination angle ( $\theta_{ax}$ ) of the radio axis with the line of sight, and the quasar emission cone. The surface of the cone coaxial with the observer's direction identifies radiation paths with the same scattering configuration. The intersection of this conical surface with the particle ellipsoid, within the quasar emission cone, at a distance  $r$  from the nucleus defines the differential volume element  $D(r, k_3)$  (thick curved line).

We assume that the radiation from the hidden quasar is confined within a cone of half opening angle  $\theta_Q$ . Since it has been shown that the observed IC emission depends on the angle between the line of sight and the incident photon beam, in order to carry out the model computations it is convenient to introduce a mean emitted power per unit solid angle and energy interval along the line of sight as:

$$< \frac{dW(r)}{dt d\epsilon_1 d\Omega_{SC}} > = \int \frac{D(r, k_3)}{[\int D(r, k_3) dk_3]} \frac{dW(r, k_3)}{dt d\epsilon_1 d\Omega_{SC}} dk_3 \quad (\text{B23})$$

where  $D(r, k_3) dk_3$  is the volume element at a distance  $r$  from the nucleus with a given  $\theta_{SC}$ . Under the assumption of an ellipsoidal distribution of the relativistic particles we find (Fig.4):

$$D(r, k_3) = \pi - 2 \arcsin \left( \frac{\cos \theta_{Q,r} - k_3 \cos \theta_{ax}}{\sin \theta_{ax} \sqrt{1 - k_3^2}} \right) \quad (\text{B24})$$

with

$$\left| \frac{\cos \theta_{Q,r} - k_3 \cos \theta_{ax}}{\sin \theta_{ax} \sqrt{1 - k_3^2}} \right| < 1$$

where  $\theta_{ax}$  is the angle between the line of sight and the radio-axis and  $\theta_{Q,r}$  is the half opening angle at a distance

$r$  from the nucleus of the quasar emission cone filled by the relativistic particles ( $\theta_{Q,r} < \theta_Q$ ).

The total IC emission has been obtained by integrating the mean emitted power (B23, B24) over all the quasar emission cone ( $\theta_Q = 45^\circ$ ) under the assumption of an uniform distribution of the relativistic electrons. The IC emission of a radio lobe along the line of sight is illustrated in **Fig. 5** as function of  $\theta_{ax}$  and for three values of  $\delta$ . This allows a quick estimate of the ratio of the emissions from the two lobes as a function of the inclination angle.

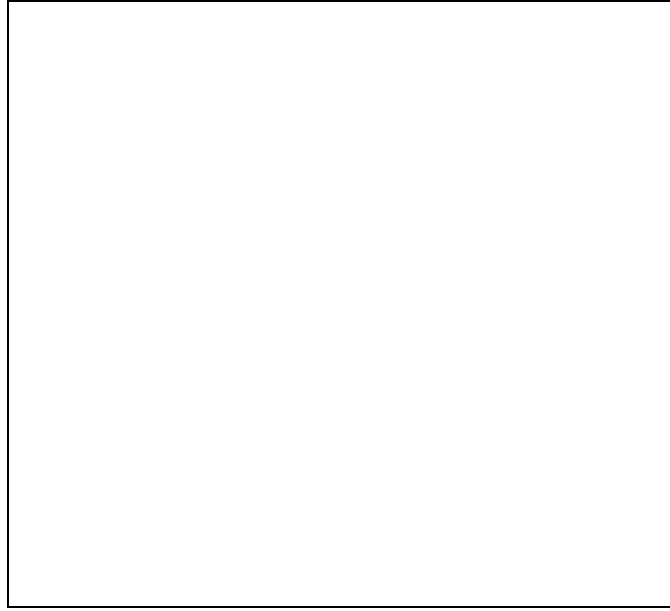
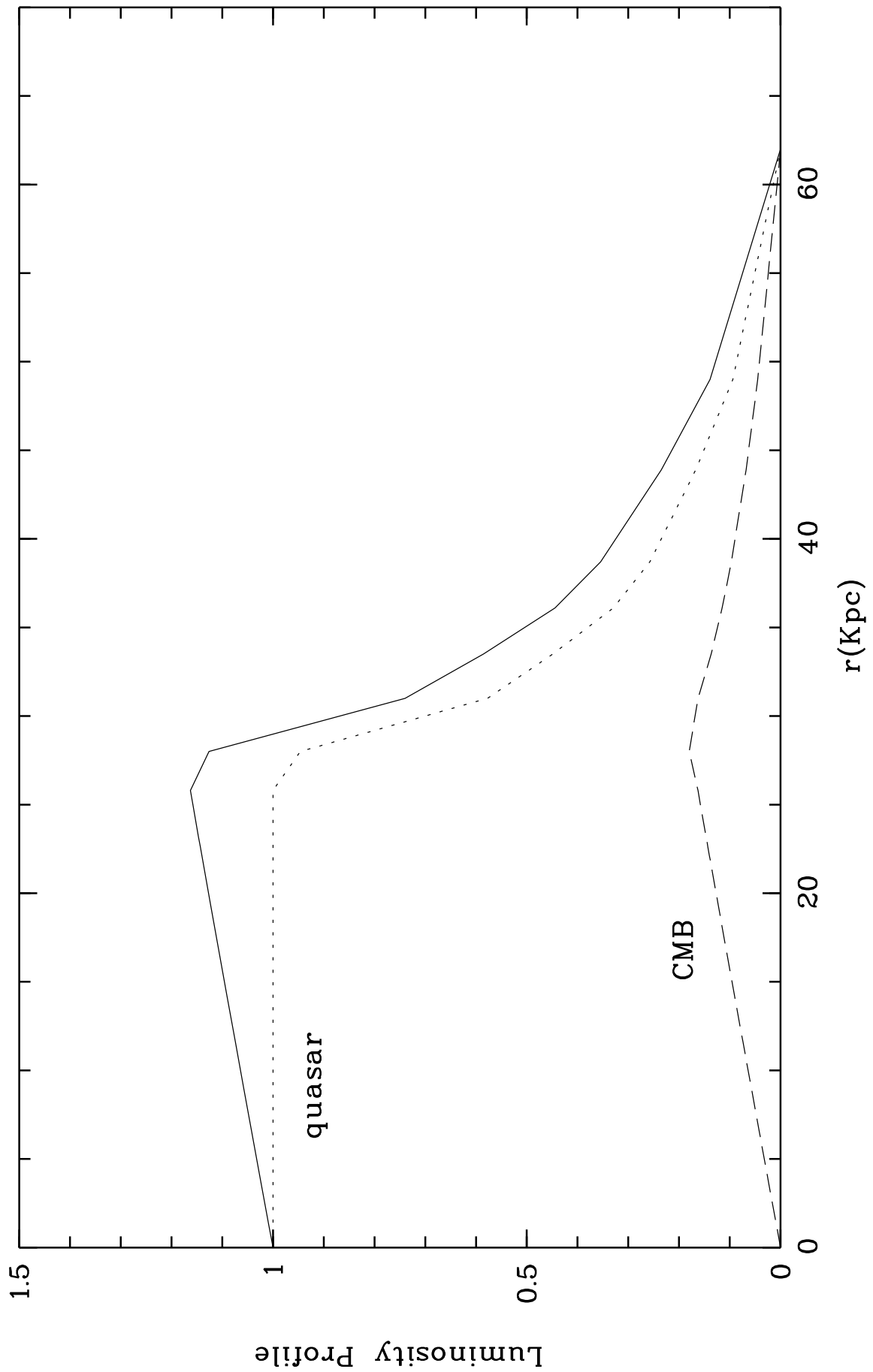


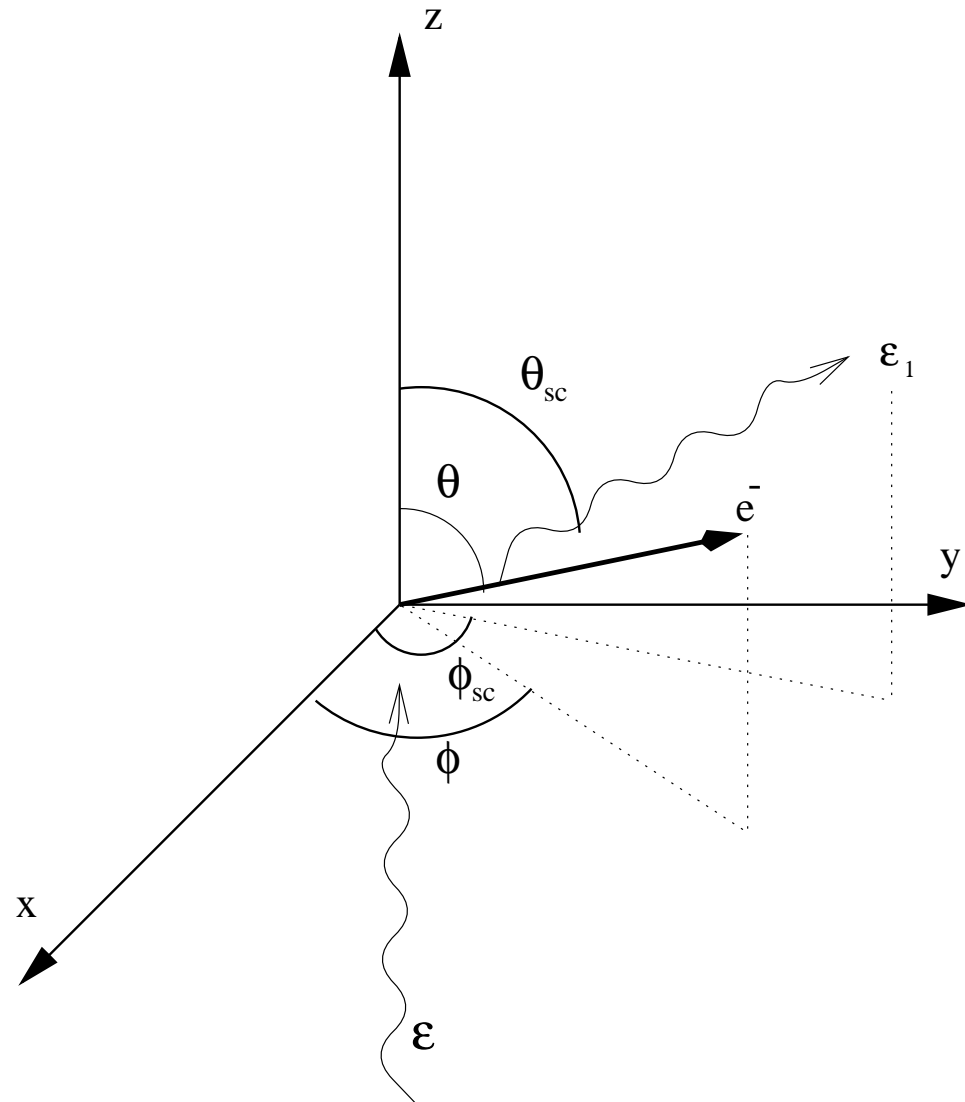
**Fig. 5.** The IC X-ray luminosity (at 1 keV) of one lobe of a radio galaxy as function of the inclination angle  $\theta_{ax}$ . The luminosity is normalized to the isotropic IC value for the same lobe and is plotted for three representative values of the electron spectral index  $\delta$ : 2.1 (solid line), 2.5 (dotted line) and 3.1 (dashed line). The computation has been performed assuming a typical ellipsoidal configuration  $100 \times 50$  Kpc and a quasar emission cone half opening angle of 45 degrees. The ratio between the luminosities of the two lobes can be easily derived from the plots keeping in mind that the lobes are symmetrically placed with respect to  $\theta_{ax} = 90^\circ$ .

## References

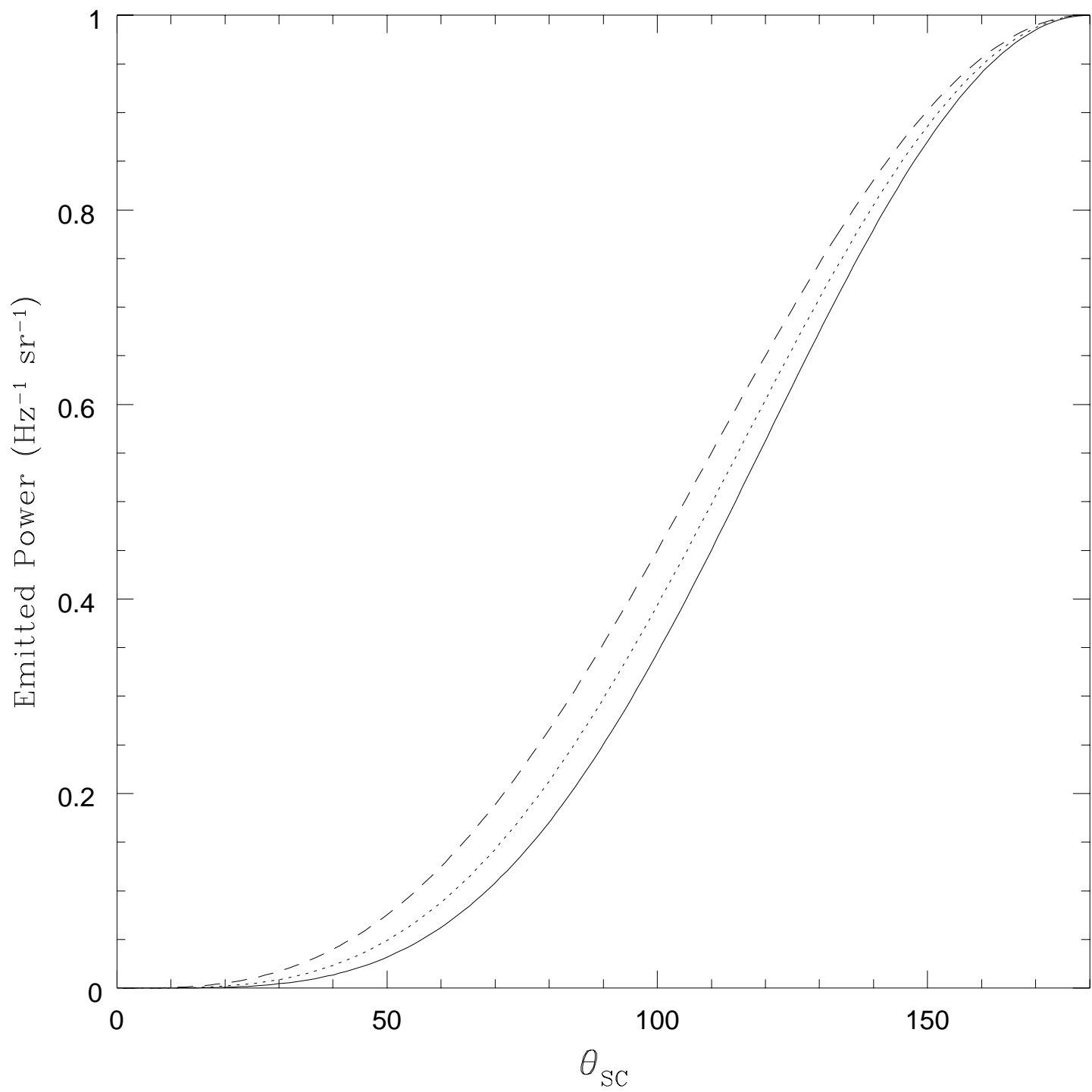
Alexander P., Leahy J.P., 1987, MNRAS 225, 1  
 Allen W., Fabian A.C., 1992, MNRAS 258, 29P  
 Antonucci R., Hurt T., Kinney A., 1994, Nature 371, 313  
 Arnaud K.A., 1987, BAAS 19, 696  
 Barthel P.D., 1989, ApJ 336, 606  
 Blumenthal G.R., Gould R.J., 1970, Rev. of Mod. Phys. 42, 237  
 Browne W.A., Murphy V., 1987, MNRAS 226, 601  
 Carilli C.L., Perley R.A., Dreher J.W., Leahy J.P., 1991, ApJ 383, 554  
 Carilli C.L., Perley R.A., Harris D.E., 1994, MNRAS 270, 173  
 Chambers K.C., Miley G.K., Joyce R.R., 1988, ApJ 329, 75  
 Cimatti A., di Serego Alighieri S., Fosbury R.A.E., Salvati M., Taylor D., 1993, MNRAS 264, 421  
 Cimatti A., Dey A., van Breugel W., Antonucci R., Spinrad H., 1996 ApJ 465, 145  
 Cimatti A., Dey A., van Breugel W., Hurt T., Antonucci R., ApJ, in press, 20 February 1997 issue  
 Crawford C.S., Fabian A.C., 1993, MNRAS 260, L15  
 Crawford C.S., Fabian A.C., 1995, MNRAS 273, 827  
 Crawford C.S., Fabian A.C., 1996a, MNRAS 281, L5  
 Crawford C.S., Fabian A.C., 1996b, MNRAS 282, 1483  
 Dey A., Spinrad H., 1996, ApJ 450, 133  
 di Serego Alighieri S., Fosbury R.A.E., Quinn P.J., Tadhunter C.N., 1989, Nature 341, 307  
 di Serego Alighieri S., Cimatti A., Fosbury R.A.E., 1993, ApJ 404, 584  
 di Serego Alighieri S., Cimatti A., Fosbury R.A.E., 1994, ApJ 431, 123  
 Djorgovski S., Spinrad H., Pedelty J., Rudnick L., Stockton A., 1987, AJ 93, 1307  
 Fabbiano G., Miller L., Trinchieri G., Longair M., Elvis M., 1984, ApJ 277, 115  
 Feigelson E.D., Laurent-Muehleisen S.A., Kollgaard R.I., Fomalont E.B., 1995, ApJ 449, L149  
 Fernini L., Burns J.O., Bridle A.H., Perley R.A., 1993, AJ 105, 1690  
 Garrington S.T., Conway R.G., 1991, MNRAS 250, 198  
 Harris D.E., Grindlay J.E., 1979, MNRAS 188, 25  
 Harris D.E., Carilli C.L., Perley L.A., 1994a, Nature 367, 713  
 Harris D.E., Perley R.A., Carilli C.L., 1994b, X-ray detection of the nuclear source in the Cygnus A galaxy. In: Courvoiser T. J.-L. and Blecha A. (eds.) Proc. IAU Symp. 159, Multi-Wavelength Continuum Emission of AGN.  
 Heckman T.M., Chambers K.C., Postman M., 1992, ApJ 391, 39  
 Heckman T.M., O'Dea C.P., Baum S.A., Laurikainen E., 1994, ApJ 428, 65  
 Herbig T., Readhead A.C.S., 1992, ApJS 81, 83  
 Hes R., Barthel P.D., Hoekstra H., 1995, A&A 303, 8  
 Hill G.J., Lilly S.J., 1991, ApJ 367, 1  
 Jones F.C., 1968, Phys. Rev. 167, 1159  
 Kaneda H. et al. 1995, ApJ 453, L13  
 Kardashev N.S., 1962, SvA 6, 317  
 Laing R.A., Riley J.M., Longair M.S., 1983, MNRAS 204, 151  
 Leahy J.P., Muxlow T.W.B., Stephens P.W., 1989, MNRAS 239, 401  
 Manzini A., di Serego Alighieri S., 1996, A&A 311, 79  
 McCarthy P.J., 1993, ARA&A 31, 639  
 McCarthy P.J., Spinrad H., Van Breugel W., et al., 1990, ApJ 365, 487  
 McCarthy P.J., Spinrad H., Van Breugel W., 1995, ApJS 99, 27  
 Meisenheimer K., Hippeltein H., 1992, A&A 264, 455  
 Pacholczyk A.G., "Radio Astrophysics", 1970, Freeman Eds.  
 Pedelty J.A., Rudnick L., McCarthy P.J., Spinrad H., 1989, AJ 97, 647  
 Pier E.A., Krolik J.H., 1992, ApJ 401, 99  
 Ronghui L., Pooley G., Riley J.M., 1992, MNRAS 257, 545L  
 Rybicki G.B., Lightman A.P., "Radiative Processes in Astrophysics", 1979, John Wiley & Sons Eds.

Sanders D.B., Phinney E.S., Neugebauer G., Soifer B.T.,  
Matthews K., 1989, ApJ 347, 29  
Spinrad H., Djorgovski S., Marr J., Aguilar L., 1985, PASP 97,  
932  
Stockton A., Ridgway S.E., Kellogg M., 1996, AJ 1689, 902  
Strom R.G., Riley J.M., Spinrad H., et al., 1990, A&A 227, 19  
Ueno S., Koyama K., Nishida M., 1994, ApJ 431, L1  
Worrall D.M., Lawrence C.R., Pearson T.J., Readhead A.C.S.,  
1994, ApJ 420L, 17  
Yates M.G., Miller L., Peacock J.A., 1989, MNRAS 240, 129

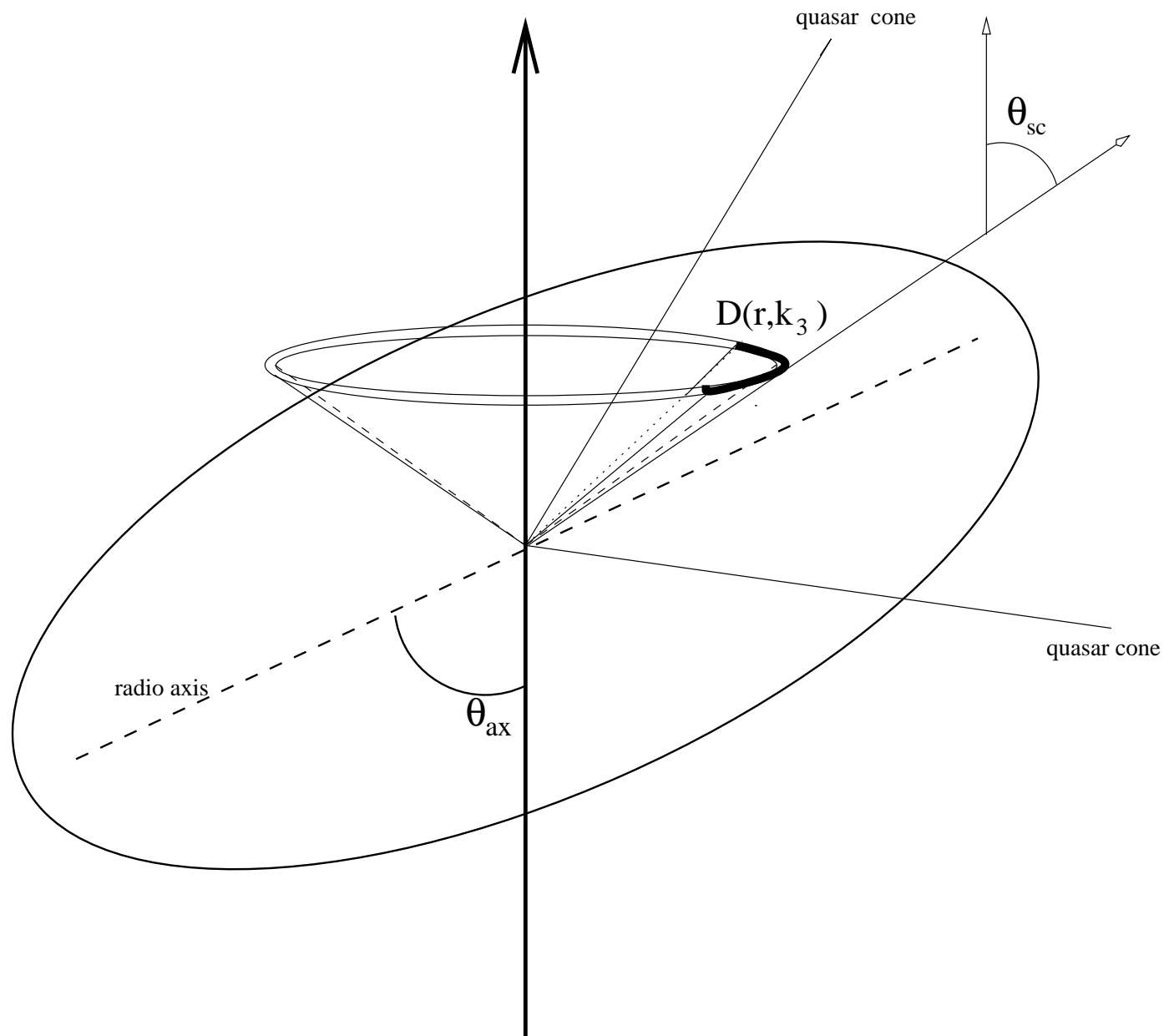








# OBSERVER





Lobe Emission

